DOI: 10.24352/UB.OVGU-2018-031 TECHNISCHE MECHANIK, 38, 3, (2018), 233 – 245
submitted: December 11, 2017

3D-Measurements of 3D-Deformations of Pantographic Structures

G. Ganzosch, K. Hoschke, T. Lekszycki, I. Giorgio, E. Turco, W. H. Müller

Samples of differently sized so-called pantographic structures are subjected to large deformation loading tests up to rupture, while their response to the deformation is recorded by an optical 3D-measurement system. Digital image correlation is used to calculate the deformation that took place perpendicular to the reference plane by the help of a four-camera system. Results show that the deformation behavior is strongly non-linear and that the structures are capable to perform large (elastic) deformations without leading to complete failure.

1 Introduction

The progress in 3D-printing technology enables the development of new structures with extraordinary geometric and mechanical characteristics (dell'Isola et al., 2016d). In combination with specially treated materials, a new class of intelligent structures was developed (dell'Isola et al., 2015b, 2016a,c). So-called Pantographic Structures (PSs) were conceived by dell'Isola, Lekszycki and their co-workers (Battista et al., 2017; Cuomo et al., 2017; dell'Isola et al., 2017, 2016b; Giorgio et al., 2016; Placidi et al., 2016; Spagnuolo et al., 2017; Turco et al., 2017, 2016c) with the aim to find a planar body that can be enlarged without damage up to about 50 percent and still remains in the elastic range. The models proposed to describe the behavior of these kind of materials fall within the general framework of micropolar anisotropic elasticity (Auffray et al., 2015; Eremeyev and Pietraszkiewicz, 2016), and can be reduced to second gradient materials (dell'Isola et al., 2015c; Pideri and Seppecher, 1997; Dos Reis and Ganghoffer, 2012; AminPour and Rizzi, 2016; Della Corte et al., 2016) by adding proper constraints. They can be interpreted as particular cases of shells, bi-dimensional foams or, from a more general point of view, as functionally graded materials or meta-materials, if the geometry of elementary constituents is suitably designed to meet given requirements (Altenbach and Eremeyev, 2009a,b, 2014; Hendy and Turco, 2008; Turco, 1998; Alibert et al., 2003; De Masi et al., 2008, 2009). Those newly introduced structures share a very similar kinematics to woven fabrics. Therefore theoretical tools developed for reinforced composites can also be applied successfully to PSs, see, e.g., (dell'Isola and Steigmann, 2015; Steigmann and dell'Isola, 2015; Misra et al., 2015; Zeidi and Kim, 2017; Alsayednoor et al., 2017; Harrison, 2016; Launay et al., 2008; Selvadurai and Nikopour, 2012).

In order to investigate the deformation behavior of PSs in the best possible way, an optical measurement technique, to be more precise, Digital Image Correlation (DIC), will be used. This non-invasive technique is able to detect and to measure a three dimensional deformation of a surface. This pattern, in which wrinkling occurs, can also be spotted in biological systems as, e.g., the skin (Lejeune et al., 2016). Uniaxial tests, shearing tests, and torsion tests were applied to PSs. Based on experimental data the extraordinary deformation behavior of PSs will be discussed.

2 Material and Methods

Because of their complex periodic structure, the pantographic samples considered for the investigations in tension, shear, and torsion tests were manufactured with the help of a 3D-printer. Polyamide as well as aluminum powder were used as raw materials. The PS consists of rectangular beams and cylindrical pivots (see Fig. 1). 3D-models have been generated by using the commercial CAD software `SolidWorks`® (Dassault Systèmes SolidWorks Corporation, Waltham, MA 02451). STL file was transformed to a GCODE and has been used as input for the 3D-printer.

For the production of the specimen made out of polyamide (PA2200) a Formiga `P 100`® (EOS GmbH, Munich, Germany) Selective Laser Sintering (SLS) 3D-printer was used at the University of Technology, Warsaw, Poland. The aluminum specimen was manufactured on an EOS `M 400`® 3D-printer with Direct Metal Laser Sintering (DMLS) from AlSi10Mg metal powder with a 1 kW laser source at Fraunhofer EMI, Freiburg, Germany. Even

small deviations during the printing process lead to breakage and abortion of the process or pre-damage in the case of filigree structures, such as PSs. In comparison to the plastic process, for the metal fabrication a special support structure and a complicated elaborated laser exposure strategy was employed in order to avoid thermal distortions due to the higher laser powers and energy input. The specimens were positioned at a special angle with regard to the building direction in order to minimize the cross-sectional area of exposure in the layer-wise process. This very angle was also chosen in a way that the arrangements of beams and pivots ensured self-supporting. The mounting area was supported. A contour based arrangement of laser tracks was used to minimize transient deviations of the energy input due to the inertia in the optical scanning system. That approach fits the geometric characteristic of the slender beams better. In Fig. 3 aluminum specimens are shown after the small batch production. Prior to support removal and separation from the building plate, a stress relief heat treatment (2 h at 300 °C) was employed for this configuration. Deviations due to thermal stresses were prevented. Heat treatment also results in ductile behavior of the material (Mower and Long, 2016) in comparison to the as-built properties.

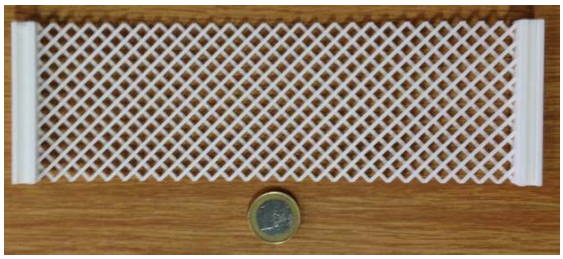

Figure 1: Polyamide sample of a PS developed by (dell'Isola et al., 2015b).

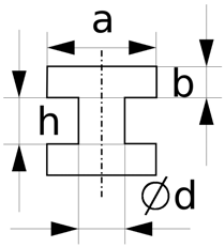

Figure 2: Example of a periodic unit cell of a PS: a and b describe width and height of a beam, Ø d and h describe diameter and height of a pivot.

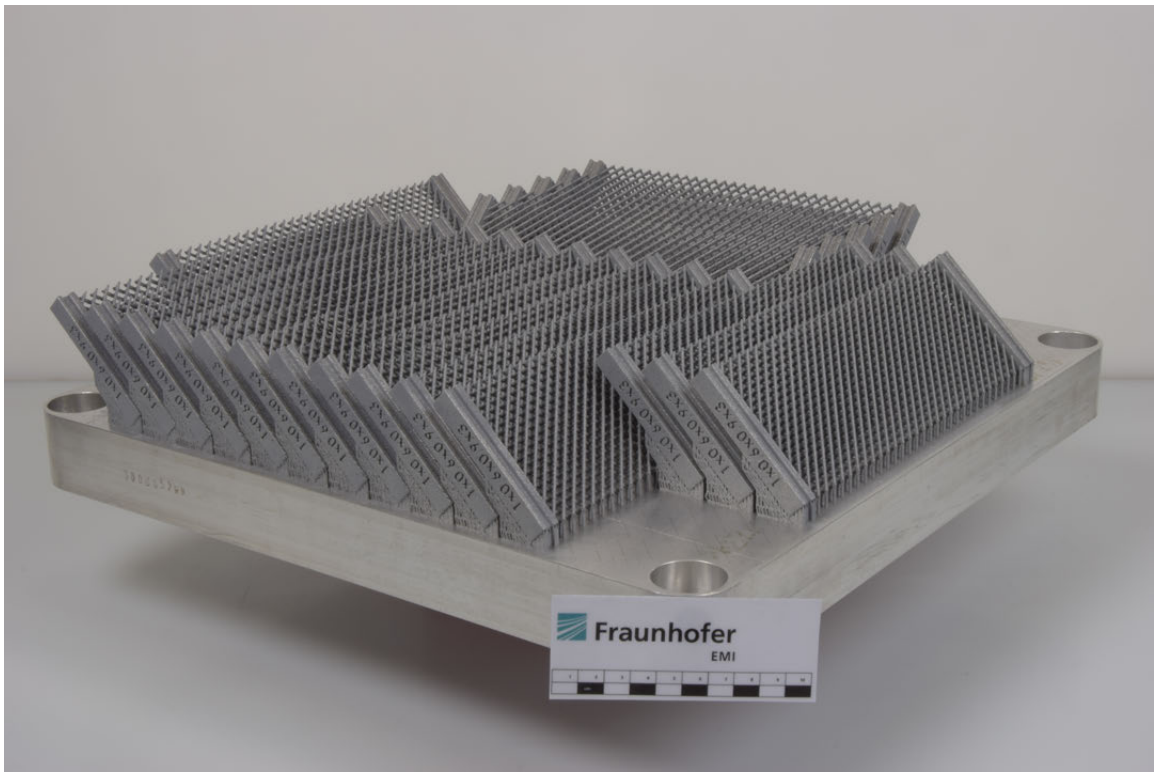

Figure 3: PSs made out of aluminum, manufactured at EMI, Freiburg, Germany.

Specimens with different internal geometries were investigated. A schematic outline of the substructure is presented in Fig. 2. It shows the different pivot parameters and beam parameters. All values of these parameters for each to be tested specimen are given in Tab. 1. The outer dimensions of all sheets are 210 mm × 70 mm. The main aim of this work is to find out if it is possible to measure surface deformation with the help of the 3D-DIC system. Furthermore, we will discuss different material parameters and their influence on the deformation behavior. Note that we will focus on shearing and torsion experiments, because out-of-plane movement was not measured in

regular tension tests. Uniaxial experiments on PSs were discussed intensively in (dell'Isola et al., 2015b, 2016a).

Sample	Material	a [mm]	b [mm]	Ø d [mm]	h [mm]
A	Polyamide	1.0	1.0	0.9	1.0
B	Aluminum	1.0	0.6	0.9	3.0

Table 1: Overview of investigated specimens: list of different materials and geometry parameters, see Fig. 2.

An overview of the experimental setup of a shearing test is shown in Fig. 4. Fig. 5 shows the setup of a torsion test. The schematic setup of the device is presented in Fig. 6. A `Zwick Z010`® testing-device, controlled by the software `TestExpert`®, was used during all tests.

The resultant applied axial force was measured by a device-own load cell (`Zwick-Serie Xforce`®). The force transducer is able to record axial forces in the range of about $\pm 10{,}000$ N, whereas the accuracy at 20 N is 0.1%. The displacement Δx was controlled vertically. The upper traverse-part of the tensile-to-shear adaption-device (see Fig. 4 and Fig. 6) is fixed horizontally and vertically, while the lower part can be linearly moved in the vertical direction. The velocity for the shear tests has been set to be 15 mm/min, what is quite slow for such tests (displacement-controlled; quasi-static). The displacement itself was recorded and monitored by a device-own encoder unit with an accuracy of $\pm 2.0\,\mu$m. For the torsion tests a device-own torque sensor (`Zwick-Serie M`®) was applied on the very fixed bottom of the lower traverse, while the torsion was induced on the top of the mounting with 1° /min on the upper traverse-part of the torque adaption-device (see Fig. 5 and Fig. 6). The torsion transducer is able to record moments up to 20 Nm and resists maximal axial forces up to $\pm 5{,}000$ N.

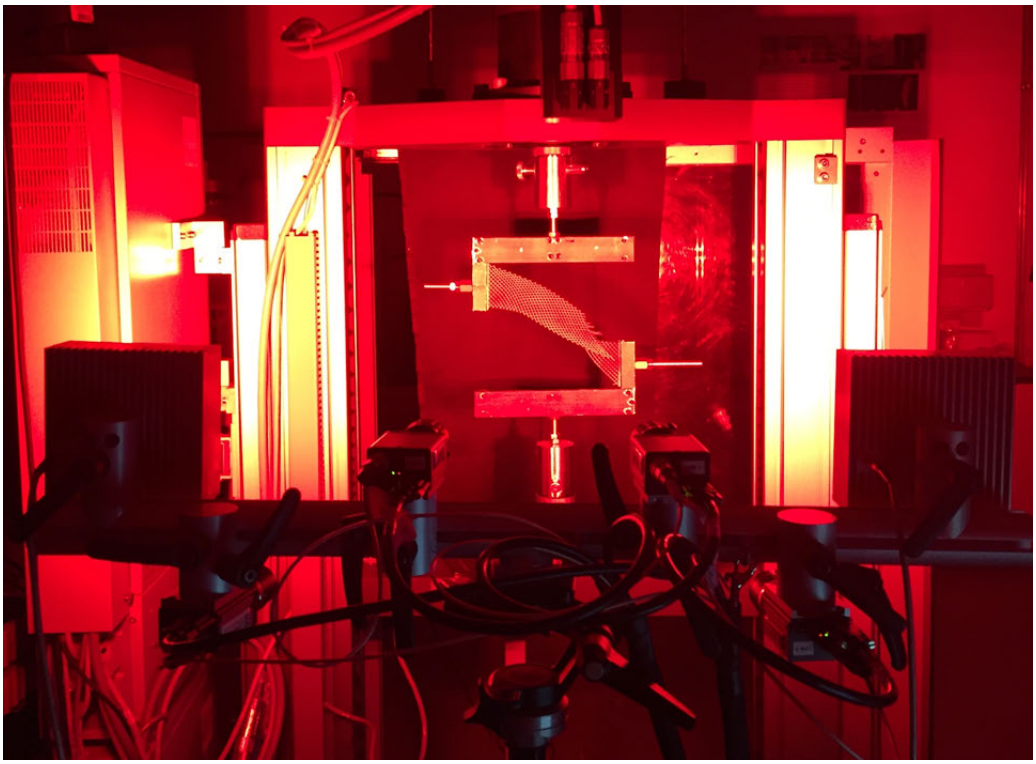

Figure 4: Experimental setup of a shear test: PS after rupture. PS is mounted into the tensile-to-shear adaption-device, which is connected to the Zwick loading machine. The upper adaption is fixed. The lower traverse can move vertically. The Dantec camera and illumination system can be recognized in the front of the figure.

A non-invasive optical measurement device `Q-400` (Dantec Dynamics GmbH, Ulm, Germany) was installed to record the state of three dimensional deformation of the surface of a sheet by the help of four cameras as shown in Fig. 4 (front) and in Fig. 5 (right). A more-than-one camera system is able to recognize the 3D-motion within overlapping regions of the image sections (in our case four cameras). Due to the large deformation applied here, this region of overlapping was doubled, in order to capture the whole deformation process. To enable the software of image correlation to separate small surface areas (so-called facets) and because of lack of contrast, the surfaces of all specimens have been sprayed in a speckled pattern using an airbrush system and the acrylic-based waterproof

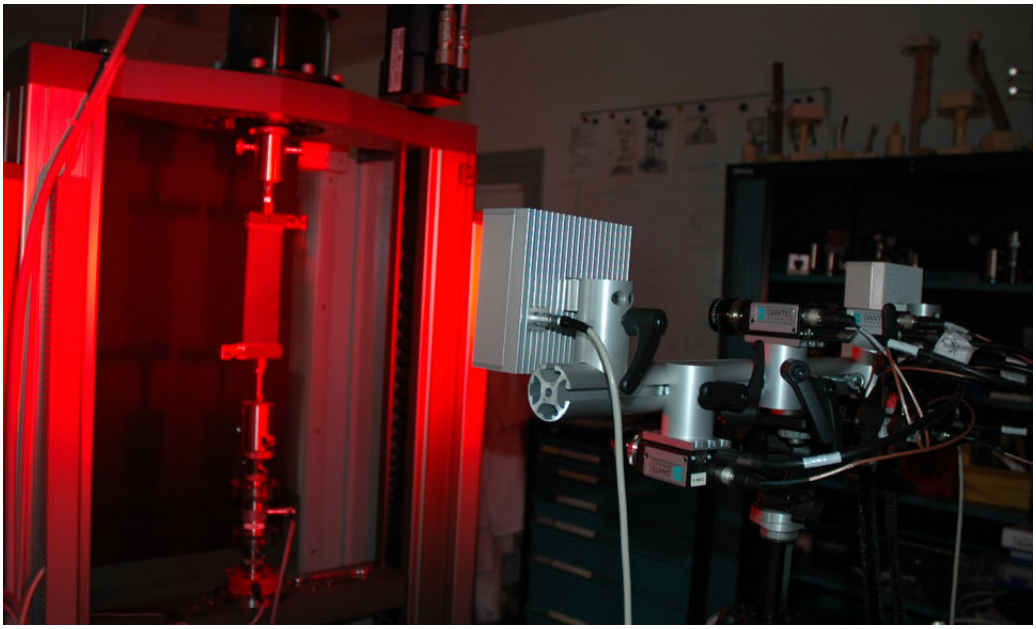

Figure 5: Experimental setup of a torsion test: PS during deformation. PS is mounted into the torsion device. The upper adaption can rotate. The lower traverse is fixed. Load-cell and torque-sensor can be recognized at the bottom. Four cameras and two illumination devices are fixed horizontally about 120 cm in front of the loading device.

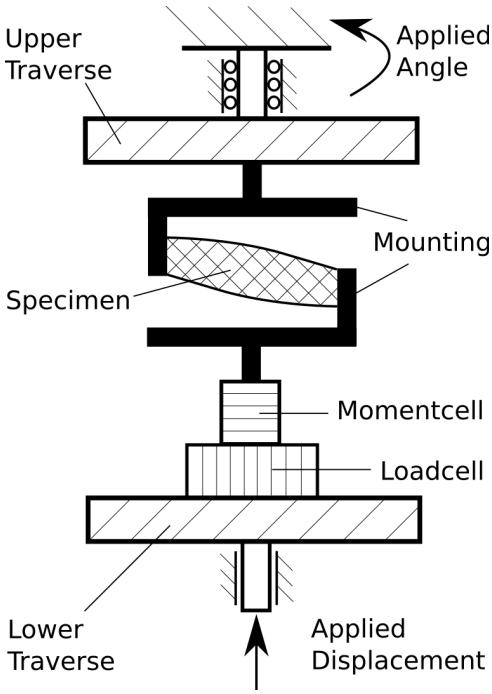

Figure 6: Schematic setup of the loading-device: Moment-cell and load-cell are fixed on the lower traverse, which is able to apply a vertical displacement. A rotation is applied aroung a fixed vertical axis from the upper traverse.

ink (Molotow One4All, Feuerstein GmbH, Lahr, Germany). During the deformation process, pictures have been taken via direct TTL-signal every 2 seconds by means of the afore mentioned commercial camera system with a resolution of about $1{,}600 \times 1{,}200$ pixels. This way, we were able to synchronize each picture to the related force-value in real time. Figure 7 shows three exemplary 2D-pictures of one of the cameras during shear test up to rupture for sample **B**. Figure 8 shows six exemplary 2D-pictures of one camera during the torsion test up to rupture for sample **B**. By means of a calibration procedure of the camera setup, the commercial software `Istra4D`® is able to re-calculate a three dimensional surface deformation.

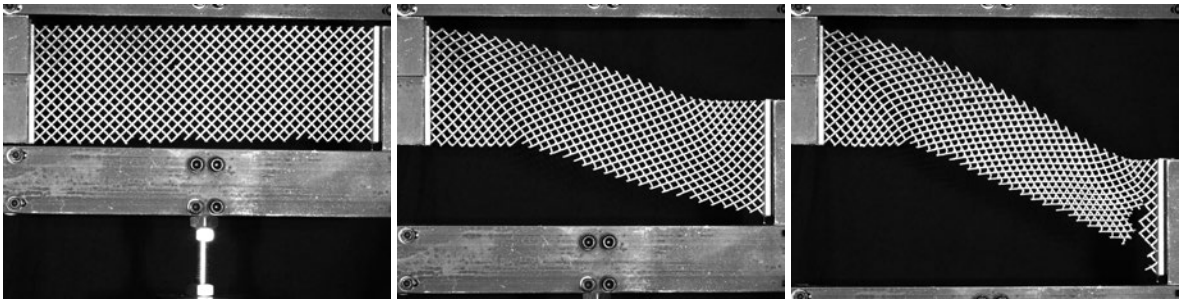

Figure 7: Exemplary raw pictures of sample **B** up to rupture during shear-load after 0 mm, 45 mm, and 80 mm shear-displacement. Rupture occurs next to the mounting in the lower right corner of the sample.

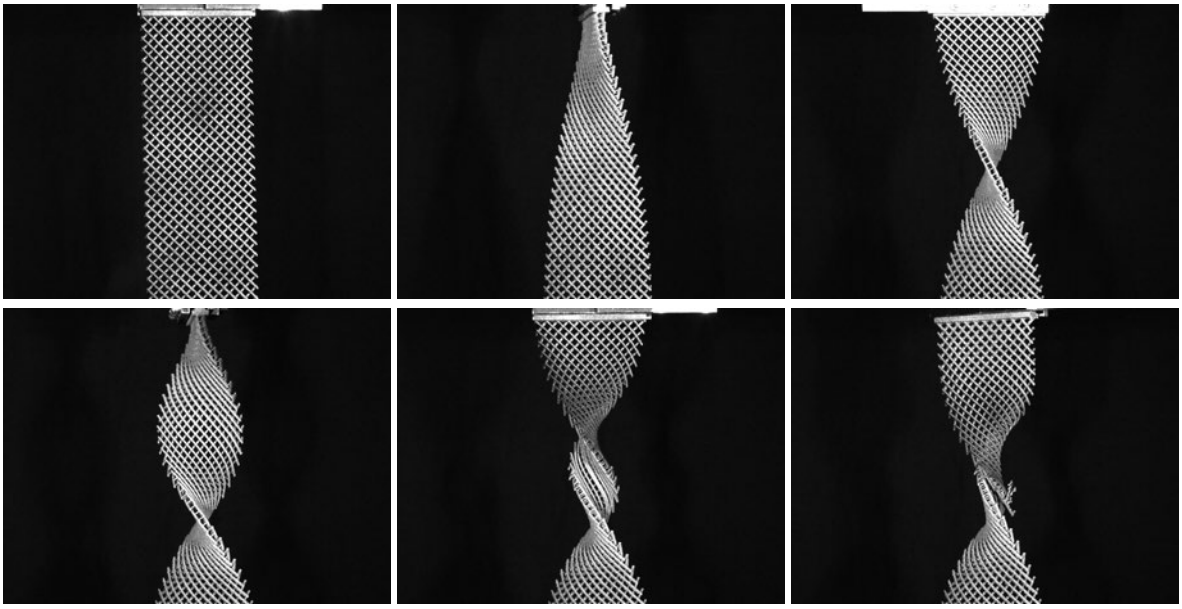

Figure 8: Exemplary raw pictures of sample **B** about every 90° (for the first five sequences) up to rupture during torsion-load. Rupture of beams can be recognized in the middle of the sheet.

Originally, the adaption-device was equipped with linear-guides, in order to ensure a parallel movement of the upper and lower part in the shearing tests. Nevertheless, the present measurements have been performed without the linear-guides in order to improve the friction induced noise signals. Results from the DIC measurements indicated that the vertical parallelism is still given, even for high loads acting on the aluminum specimen. After evaluating the 3D-data, only a minor out-of-plane movement of the lower part of the shear-adapter has been recognized and taken into account for sample **B**.

3 Results

In order to obtain scalar results for an out-of-plane displacement of a sheet, a point in a single facet (a sub-area of image correlation) has been selected for each sample. This point is located in the place where maximal out-of-plane movement has been presumed. Due to the large deformations, some facets will move out of the optical focus, which may cause the image correlation to abort. Furthermore, image correlation is aborted, when a sudden rupture occurs in between the shutter releases, so that the facets to be correlated are displaced laterally too much. For these reasons some of the facets in Fig. 11 and some plots in Fig. 9 are incomplete.

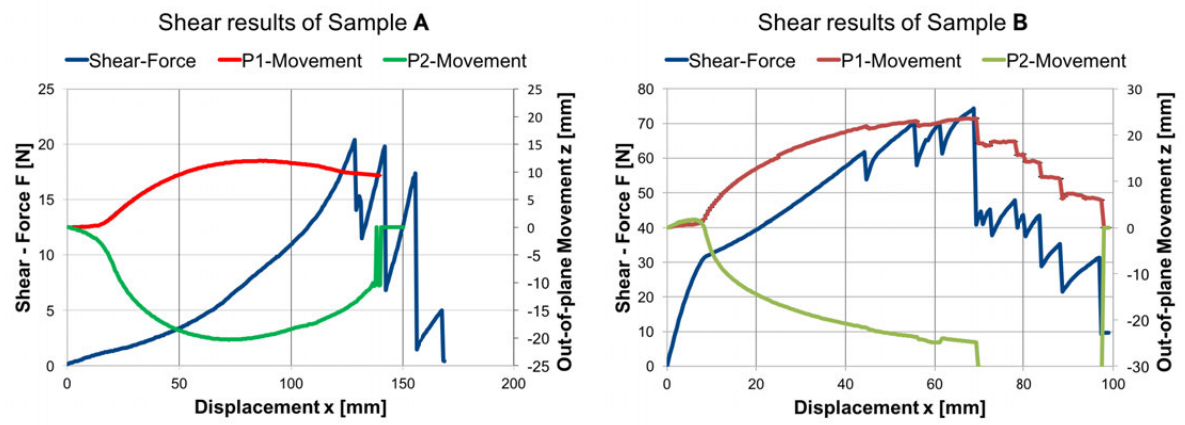

Figure 9: Shear-force/displacement diagram and out-of-plane movement/displacement diagram of sample **A** (left picture) and sample **B** (right picture) during shear-load.

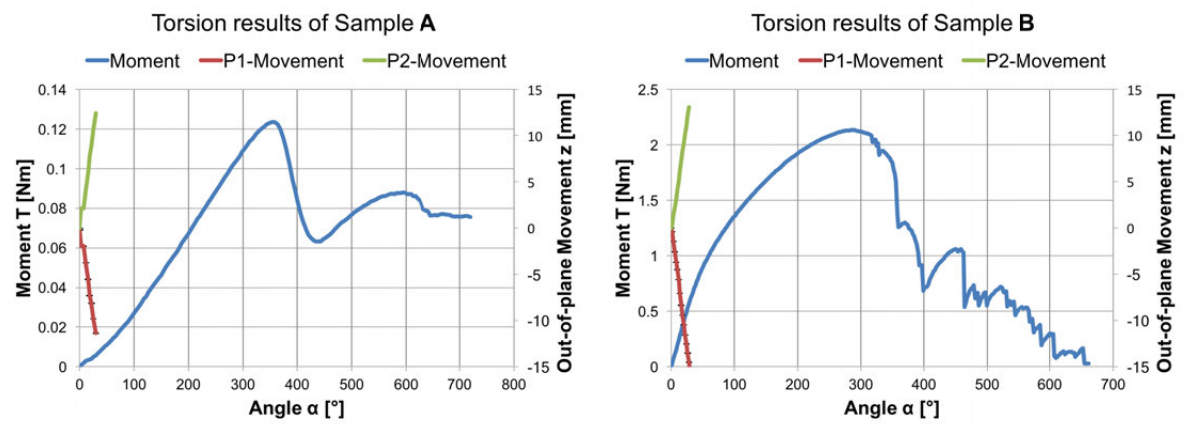

Figure 10: Moment/angle diagram and out-of-plane movement/angle diagram of sample **A** (left picture) and sample **B** (right picture) during torsion.

The summary of the experimental results of both samples, the polyamide one as well as the aluminum one, are visualized in Fig. 9 for the case of shearing, showing the plots for the shear-force vs. shear-displacement (left ordinate), as well as the out-of-plane vs. the shear-displacement (right ordinate). In Fig. 10 experimental results of both samples for the case of torsion are plotted, showing the plots for the moment vs. twist-angle (left ordinate), as well as the out-of-plane vs. the twist-angle (right ordinate). Local minima in all plots describe failure of a beam or a pivot. All samples show different and pronounced non-linear curves.

In order to demonstrate the data acquisition, Fig. 11 shows the processed 3D-data of both samples during the shear deformation. Regrading the data acquisition for the case of torsion, Fig. 12 shows the processed 3D-data of both samples during the torsional deformation. All data was generated without smoothing.

Furthermore, Table 2 shows the maximal out-of-plane displacement values per sample for shearing as well as for torsion, within the valid measurement ranges.

Sample	Maximal out-of-plane displ. in shearing-test [mm]	Maximal out-of-plane displ. in torsion-test [mm]
A	-20.31	12.39
B	-23.29	-16.27

Table 2: Maximal out-of-plane values for shearing and torsion.

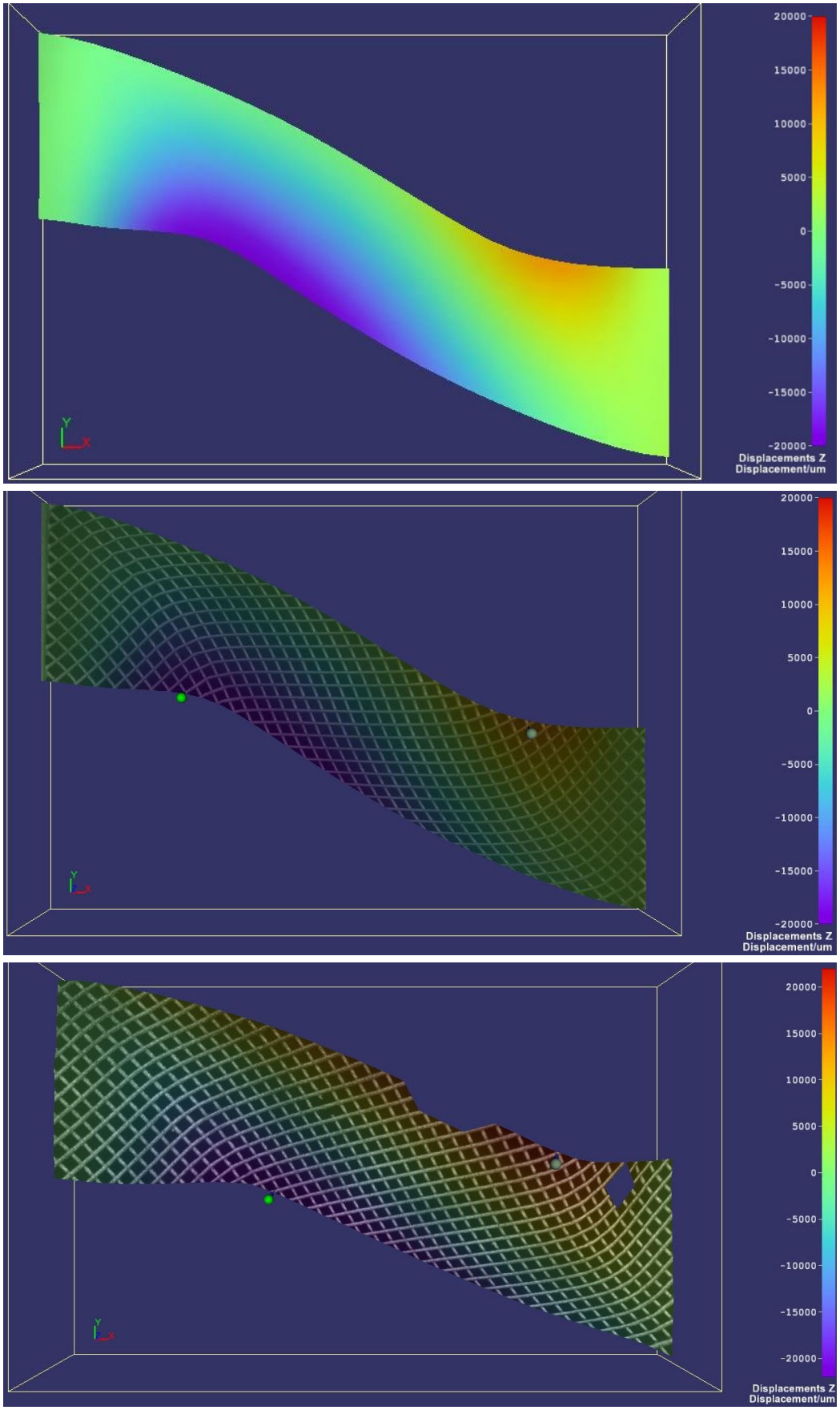

Figure 11: 3D-evaluation-image during the shearing tests: red areas in the upper right part of the sheet show out-of-plane movement in the positive direction, blue areas in the lower left part of the sheet show negative movements. Pure data of sample **A** (upper figure). Overlay with real image of sample **A** (middle figure). Overlay with real image of sample **B** (lower figure). A symmetric deformation can be observed.

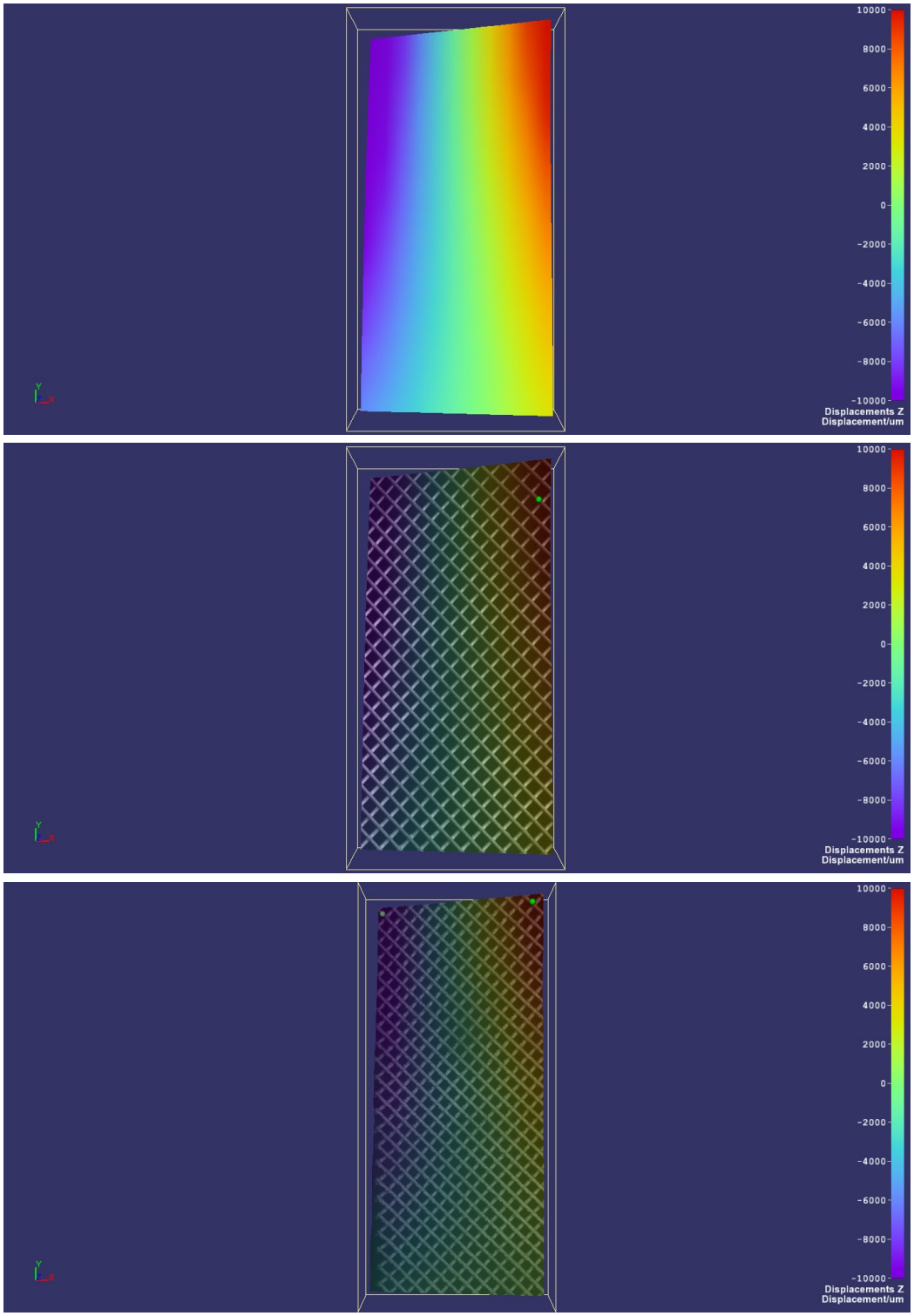

Figure 12: 3D-evaluation-image during the torsion tests: red areas in the upper right corner show out-of-plane movement in the positive direction, blue areas in the upper left corner show negative movements. Pure data of sample **A** (upper figure). Overlay with real image of sample **A** (middle figure). Overlay with real image of sample **B** (lower figure). A symmetric deformation can be observed.

4 Discussion and Conclusion

It is possible to measure out-of-plane movement of 3D-deformation applied to PSs. Furthermore, we confirmed the presumed non-linear deformation behavior, which was also measured in our preliminary work (dell'Isola et al.,

2015b; Ganzosch et al., 2017). By comparing the shear-forces of sample **A** and sample **B** in Fig. 9 (blue curve), it can be recognized that the aluminum sample **B** is able to resist outer loads about three times higher than the polyamide one until first rupture occurs. Although parameters of sample **B** are smaller than the ones of sample **A** (see Table 1), sample **B** resists higher load conditions because of the stiffer material behavior of aluminum. Both samples show non-linear deformation behaviors. At about 32 N the structure of sample **B** fails and a buckling effect occurs. Henceforth a weaker and less stiffer response to outer load can be recognized. A local minimum appears in the plot if a pivot or a beam breaks. After one failure within the structure the specimen "recovers" and is able to carry even higher loads than before. Because of the complex geometry, beams and pivots reorganize themselves resulting in a higher resistance to outer load, so that even higher loads can be carried (see sample **B**) after local failure in a beam or a pivot.

This kind of extraordinary deformation behavior was also observed in the torsion-tests (see Fig. 10). A strongly non-linear dependence of moment and angle was measured (blue curve). The maximal torsion-load of sample **B** is about seventeen times higher than the one measured for the polyamide sample **A**. Note that the maximum torque was measured for sample **A** after about one full rotation and for sample **B** at a rotation of about $280°$. These high values indicate a very robust and strong resistance to outer torsion-loads and will be discussed further in future research with a focus on specific material characteristics (Misra, 1997; Misra and Chang, 1993) and geometric non-linearity (Misra et al., 2018).

By comparing the out-of-plane movement of both samples during the shearing-test, which are marked red for positive values and green for negative values on second ordinate axis in Fig. 9, non-symmetric out-of-plane movement for the polyamide sample **A** and symmetric out-of-plane movement for the aluminum sample **B** are distinguishable. The positive out-of-plane movement of sample **A** is much smaller than the negative one. This is visualized in the upper picture and in the middle picture of Fig. 11 by the red areas for positive out-of-plane movements and by the blue areas for negative out-of-plane movements. One reason for this behavior is the manufacturing-process of the specimen. Because of the print direction in rapid-prototyping, a non-homogeneous material distribution resulting in an asymmetry of the structure is conceivable. Another reason could result from the machine compliance of the mounting device (the same one was used for all experiments). Because of the symmetric out-of-plane movement of the aluminum sample **B**, which shows much stiffer and symmetric response behavior (see lower picture of Fig. 11), the machine compliance should not be the main reason for the non-symmetric out-of-plane movement. The symmetric out-of-plane movement of sample **B** starts at about 9 mm simultaneously when the kink of the shear-force occurs. At this very point the whole structure becomes unstable, because some beams start to buckle and to twist resulting in an out-of-plane movement. Another explanation could come from the failure of pivots. After leaving the elastic range, the pivot is plastically deformed and unable to resist the shear-force resulting in a failure and therefore out-of-plane movement of the attached beams.

In Fig. 12 the positive (red areas) and negative (blue areas) out-of-plane movements are visualized for the case of torsion. By comparing the maximal out-of-plane movements of shearing with torsion in Table 2, lower values for torsion are measured. The main reason for this fact is the limitation of the camera-focus. In the very middle of the recorded picture the focus is better than in the outer corners, were the evaluated out-of-plane movement of points was measured. But still, the non-smoothed results indicate that the measured values are within an error of $\pm 10\,\mu$m.

In order to achieve more precise results in the future, a redesign of the mounting clamps has to be considered allowing to manipulate the mounting plates to ensure their parallelism. Furthermore, all parts should be manufactured with a stronger material, such as stainless steel, with the aim to reduce the compliance of the mounting device. Another source of error is the manufacturing process of the specimen. Here we suggest to optimize the process-parameters for printing machines in order to find a procedure, in which a more homogeneous specimen will be printed. Moreover, the calibration procedure between the cameras should be developed further. It is important to find the right balance between illumination settings and contrast of the speckle pattern. Based on the preliminary work of (dell'Isola et al., 2016a; Placidi et al., 2015; Barchiesi et al., 2018) we want to develop an analytical and numerical model to investigate the extraordinary deformation behavior more precisely. A key point to obtain predictive simulations is to identify the material parameters to be used in the adopted models. To address this issue the reader may refer to the recent achievements obtained in (Placidi et al., 2015, 2017b,a).

Another future development concerns the ability to describe possible interactions between beams in the cases in which these come into contact (see, e.g., Misra and Huang (2012); Andreaus et al. (2016, 2013); Misra et al. (2018)). This circumstance is very interesting because PSs, which behave like a second gradient material (dell'Isola et al., 2016c, 2015a; Eugster and dell'Isola, 2017b,a), can exhibit some sort of phase transition behavior characterized by the presence of zones behaving like a first gradient material (De Masi et al. (2006); Chatzigeorgiou et al. (2015); De Masi et al. (2011)). Furthermore, the development of models related to damage evolution and plasticity

should be taken into account for the particular nature of the system under study. To address this issue some first results are presented in (Yang and Misra, 2012; Thiagarajan and Misra, 2004; Placidi, 2016). As seen in (Turco et al., 2016b,a; Barchiesi et al., 2018) and described for other materials in (Ganzosch and Müller, 2016), results obtained from higher gradient simulations will be compared with our real experiments and investigated further. 2D-structures with 3D-deformation were considered in this work. But with the progress in 3D-prototyping, we are also able to investigate 3D-deformation of 3D-structures, which are based on pantographic sheets, in the future.

Pantographic structures show extraordinary features: the deformation behavior is strongly nonlinear, and they are able to undergo large elastic deformations without reaching complete failure (strong resilient behavior). The combination of this special deformation behavior and intelligent artificial materials, such as electroactive polymers, makes PSs very interesting for industrial applications: It is conceivable that PSs could serve as a meta-material for stents or in medical devices (because of their resilient properties) or as a protective bullet-shield for security applications.

5 Acknowledgement

We want to thank Dag Wulsten and Paul Zaslansky from the Julius Wolff Institute at Charité in Berlin, Germany, for their help and support in the lab.

References

Alibert, J.-J.; Seppecher, P.; dell'Isola, F.: Truss modular beams with deformation energy depending on higher displacement gradients. *Mathematics and Mechanics of Solids*, 8, 1, (2003), 51–73.

Alsayednoor, J.; Lennard, F.; Yu, W.; Harrison, P.: Influence of specimen pre-shear and wrinkling on the accuracy of uniaxial bias extension test results. *Composites Part A: Applied Science and Manufacturing*, 101, (2017), 81–97.

Altenbach, H.; Eremeyev, V.: Eigen-vibrations of plates made of functionally graded material. *Computers, Materials, & Continua*, 9, 2, (2009a), 153–178.

Altenbach, H.; Eremeyev, V. A.: On the bending of viscoelastic plates made of polymer foams. *Acta Mechanica*, 204, 3-4, (2009b), 137.

Altenbach, H.; Eremeyev, V. A.: Vibration analysis of non-linear 6-parameter prestressed shells. *Meccanica*, 49, 8, (2014), 1751–1761.

AminPour, H.; Rizzi, N.: A one-dimensional continuum with microstructure for single-wall carbon nanotubes bifurcation analysis. *Mathematics and Mechanics of Solids*, 21, 2, (2016), 168–181.

Andreaus, U.; Baragatti, P.; Placidi, L.: Experimental and numerical investigations of the responses of a cantilever beam possibly contacting a deformable and dissipative obstacle under harmonic excitation. *International Journal of Non-Linear Mechanics*, 80, (2016), 96–106.

Andreaus, U.; Placidi, L.; Rega, G.: Microcantilever dynamics in tapping mode atomic force microscopy via higher eigenmodes analysis. *Journal of Applied Physics*, 113, 22, (2013), 224–302.

Auffray, N.; Dirrenberger, J.; Rosi, G.: A complete description of bi-dimensional anisotropic strain-gradient elasticity. *International Journal of Solids and Structures*, 69, (2015), 195–206.

Barchiesi, E.; Ganzosch, G.; Liebold, C.; Placidi, L.; Grygoruk, R.; Müller, W. H.: Out-of-plane buckling of pantographic fabrics in displacement-controlled shear tests: experimental results and model validation. *Continuum Mechanics and Thermodynamics*.

Battista, A.; Del Vescovo, D.; Rizzi, N.; Turco, E.: Frequency shifts in natural vibrations in pantographic metamaterials under biaxial tests. *Technische Mechanik*, 37, 1, (2017), 17.

Chatzigeorgiou, G.; Javili, A.; Steinmann, P.: Multiscale modelling for composites with energetic interfaces at the micro-or nanoscale. *Mathematics and Mechanics of Solids*, 20, 9, (2015), 1130–1145.

Cuomo, M.; dell'Isola, F.; Greco, L.; Rizzi, N.: First versus second gradient energies for planar sheets with two families of inextensible fibres: Investigation on deformation boundary layers, discontinuities and geometrical instabilities. *Composites Part B: Engineering*, 115, (2017), 423–448.

De Masi, A.; Dirr, N.; Presutti, E.: Interface instability under forced displacements. In: *Annales Henri Poincaré*, vol. 7, pages 471–511, Springer (2006).

De Masi, A.; Merola, I.; Presutti, E.; Vignaud, Y.: Potts models in the continuum. uniqueness and exponential decay in the restricted ensembles. *Journal of Statistical Physics*, 133, 2, (2008), 281–345.

De Masi, A.; Merola, I.; Presutti, E.; Vignaud, Y.: Coexistence of ordered and disordered phases in potts models in the continuum. *Journal of Statistical Physics*, 134, 2, (2009), 243–306.

De Masi, A.; Presutti, E.; Tsagkarogiannis, D.: Fourier law, phase transitions and the stationary stefan problem. *Archive for rational mechanics and analysis*, 201, 2, (2011), 681–725.

Della Corte, A.; dell'Isola, F.; Esposito, R.; Pulvirenti, M.: Equilibria of a clamped euler beam (elastica) with distributed load: Large deformations. *Mathematical Models and Methods in Applied Sciences*, pages 1–31.

dell'Isola, F.; Andreaus, U.; Placidi, L.: At the origins and in the vanguard of peridynamics, non-local and higher-gradient continuum mechanics: An underestimated and still topical contribution of Gabrio Piola. *Mathematics and Mechanics of Solids*, 20, 8, (2015a), 887–928.

dell'Isola, F.; Cuomo, M.; Greco, L.; Della Corte, A.: Bias extension test for pantographic sheets: numerical simulations based on second gradient shear energies. *Journal of Engineering Mathematics*, 103, 1, (2017), 127–157.

dell'Isola, F.; Della Corte, A.; Giorgio, I.; Scerrato, D.: Pantographic 2D sheets: Discussion of some numerical investigations and potential applications. *International Journal of Non-Linear Mechanics, Elsevier*, 80, (2016a), 200–208.

dell'Isola, F.; Della Corte, A.; Greco, L.; Luongo, A.: Plane bias extension test for a continuum with two inextensible families of fibers: A variational treatment with lagrange multipliers and a perturbation solution. *International Journal of Solids and Structures*, 81, (2016b), 1–12.

dell'Isola, F.; Giorgio, I.; Pawlikowski, M.; Rizzi, N.: Large deformations of planar extensible beams and pantographic lattices: heuristic homogenization, experimental and numerical examples of equilibrium. 472, 2185, (2016c), 790.

dell'Isola, F.; Lekszycki, T.; Pawlikowski, M.; Grygoruk, R.; Greco, L.: Designing a light fabric metamaterial being highly macroscopically tough under directional extension: First experimental evidence. *Zeitschrift für angewandte Mathematik und Physik, ZAMP*, 66, 6, (2015b), 3473–3498.

dell'Isola, F.; Seppecher, P.; Della Corte, A.: The postulations á la d'alembert and á la cauchy for higher gradient continuum theories are equivalent: a review of existing results. 471, 2183, (2015c), 415.

dell'Isola, F.; Steigmann, D.: A two-dimensional gradient-elasticity theory for woven fabrics. *Journal of Elasticity*, 118, 1, (2015), 113–125.

dell'Isola, F.; Steigmann, D.; Della Corte, A.: Synthesis of fibrous complex structures: designing microstructure to deliver targeted macroscale response. *Applied Mechanics Reviews*, 67, 6, (2016d), 21.

Dos Reis, F.; Ganghoffer, J.: Construction of micropolar continua from the asymptotic homogenization of beam lattices. *Computers & Structures*, 112, (2012), 354–363.

Eremeyev, V. A.; Pietraszkiewicz, W.: Material symmetry group and constitutive equations of micropolar anisotropic elastic solids. *Mathematics and Mechanics of Solids*, 21, 2, (2016), 210–221.

Eugster, S. R.; dell'Isola, F.: Exegesis of sect. ii and iii. a from "fundamentals of the mechanics of continua". *Zeitschrift für Angewandte Mathematik und Mechanik*.

Eugster, S. R.; dell'Isola, F.: Exegesis of the introduction and sect. i from "fundamentals of the mechanics of continua". *Zeitschrift für Angewandte Mathematik und Mechanik*, 97, 4, (2017b), 477–506.

Ganzosch, G.; dell'Isola, F.; Turco, E.; Lekszycki, T.; Müller, W.: Shearing tests applied to pantographic structures. *Acta Polytechnica CTU Proceedings*, 7, 1–6.

Ganzosch, G.; Müller, W. H.: Experimental techniques applied to generalized continuum theories - a state-of-the-art report. *Proceedings of the XLIV Summer School-Conference Advanced Problems in Mechanics, APM, St. Petersburg, Russia*, 44, (2016), 149–161.

Giorgio, I.; Della Corte, A.; dell'Isola, F.; Steigmann, D. J.: Buckling modes in pantographic lattices. *Comptes Rendus Mecanique*, 344, 7, (2016), 487–501.

Harrison, P.: Modelling the forming mechanics of engineering fabrics using a mutually constrained pantographic beam and membrane mesh. *Composites Part A: Applied Science and Manufacturing*, 81, (2016), 145–157.

Hendy, C. R.; Turco, E.: Numerical validation of simplified theories for design rules of transversely stiffened plate girders. *Structural Engineer*, 86, 21, (2008), 37–46.

Launay, J.; Hivet, G.; Duong, A. V.; Boisse, P.: Experimental analysis of the influence of tensions on in plane shear behaviour of woven composite reinforcements. *Composites science and technology*, 68, 2, (2008), 506–515.

Lejeune, E.; Javili, A.; Linder, C.: An algorithmic approach to multi-layer wrinkling. *Extreme Mechanics Letters*, 7, (2016), 10–17.

Misra, A.: Mechanist Model for Contact Between Rough Surfaces. *Journal of Engineering Mechanics*, 123, 5, (1997), 475–484.

Misra, A.; Chang, C. S.: Effective elastic moduli of heterogeneous granular solids. *International Journal of Solids and Structures*, 30, 18, (1993), 2547–2566.

Misra, A.; Huang, S.: Micromechanical stress–displacement model for rough interfaces: Effect of asperity contact orientation on closure and shear behavior. *International Journal of Solids and Structures*, 49, 1, (2012), 111–120.

Misra, A.; Lekszycki, T.; Giorgio, I.; Ganzosch, G.; Müller, W. H.; dell'Isola, F.: Pantographic metamaterials show atypical poynting effect reversal. *Mechanics Research Communications*, 89, (2018), 6 – 10.

Misra, A.; Parthasarathy, R.; Singh, V.; Spencer, P.: Micro-poromechanics model of fluid-saturated chemically active fibrous media. *ZAMM-Journal of Applied Mathematics and Mechanics/Zeitschrift für Angewandte Mathematik und Mechanik*, 95, 2, (2015), 215–234.

Mower, T.; Long, M.: Mechanical behavior of additive manufactured, powder-bed laser-fused materials. *Material Science and Engineering A*, 651, (2016), 198–213.

Pideri, C.; Seppecher, P.: A second gradient material resulting from the homogenization of an heterogeneous linear elastic medium. *Continuum Mechanics and Thermodynamics*, 9, 5, (1997), 241–257.

Placidi, L.: A variational approach for a nonlinear one-dimensional damage-elasto-plastic second-gradient continuum model. *Continuum Mechanics and Thermodynamics*, 28, 1-2, (2016), 119–137.

Placidi, L.; Andreaus, U.; Della Corte, A.; Lekszycki, T.: Gedanken experiments for the determination of two-dimensional linear second gradient elasticity coefficients. *Zeitschrift für angewandte Mathematik und Physik, ZAMP*, 66, 6, (2015), 3699–3725.

Placidi, L.; Barchiesi, E.; Battista, A.: An inverse method to get further analytical solutions for a class of metamaterials aimed to validate numerical integrations. In: *Mathematical Modelling in Solid Mechanics*, pages 193–210, Springer (2017a).

Placidi, L.; Barchiesi, E.; Della Corte, A.: Identification of two-dimensional pantographic structures with a linear d4 orthotropic second gradient elastic model accounting for external bulk double forces. In: *Mathematical Modelling in Solid Mechanics*, pages 211–232, Springer (2017b).

Placidi, L.; Barchiesi, E.; Turco, E.; Rizzi, N. L.: A review on 2D models for the description of pantographic fabrics. *Zeitschrift für angewandte Mathematik und Physik*, 67, 5, (2016), 121.

Selvadurai, A.; Nikopour, H.: Transverse elasticity of a unidirectionally reinforced composite with an irregular fibre arrangement: experiments, theory and computations. *Composite Structures*, 94, 6, (2012), 1973–1981.

Spagnuolo, M.; Barcz, K.; Pfaff, A.; dell'Isola, F.; Franciosi, P.: Qualitative pivot damage analysis in aluminum printed pantographic sheets: numerics and experiments. *Mechanics Research Communications*, pages 47–52.

Steigmann, D. J.; dell'Isola, F.: Mechanical response of fabric sheets to three-dimensional bending, twisting, and stretching. *Acta Mechanica Sinica*, 31, 3, (2015), 373–382.

Thiagarajan, G.; Misra, A.: Fracture simulation for anisotropic materials using a virtual internal bond model. *International Journal of Solids and Structures*, 41, 11, (2004), 2919–2938.

Turco, E.: Load distribution modelling for pin-jointed trusses by an inverse approach. *Computer Methods in Applied Mechanics and Engineering*, 165, 1-4, (1998), 291–306.

Turco, E.; dell'Isola, F.; Cazzani, A.; Rizzi, N.: Hencky-type discrete model for pantographic structures: numerical comparison with second gradient continuum models. *Zeitschrift für angewandte Mathematik und Physik, ZAMP*, 67, 85, (2016a), 1–28.

Turco, E.; dell'Isola, F.; Rizzi, N.; Grygoruk, R.; Müller, W.; Liebold, C.: Fiber rupture in sheared planar pantographic sheets: Numerical and experimental evidence. *Mechanics Research Communications, Elsevier*, 76, (2016b), 86–90.

Turco, E.; Giorgio, I.; Misra, A.; dell'Isola, F.: King post truss as a motif for internal structure of (meta)material with controlled elastic properties. *Royal Society Open Science*, 4, (2017), 20.

Turco, E.; Golaszewski, M.; Cazzani, A.; Rizzi, N. L.: Large deformations induced in planar pantographic sheets by loads applied on fibers: experimental validation of a discrete lagrangian model. *Mechanics Research Communications*, 76, (2016c), 51–56.

Yang, Y.; Misra, A.: Micromechanics based second gradient continuum theory for shear band modeling in cohesive granular materials following damage elasticity. *International Journal of Solids and Structures*, 49, 18, (2012), 2500–2514.

Zeidi, M.; Kim, C. I.: Mechanics of fiber composites with fibers resistant to extension and flexure. *Mathematics and Mechanics of Solids*.

Address: Gregor Ganzosch, Technische Universität Berlin,
Institut für Mechanik, Fachgebiet Kontinuumsmechanik und Materialtheorie,
Sekr. MS2, Einsteinufer 5, 10587 Berlin, Germany
email: `ganzosch@tu-berlin.de`

Address: Klaus Hoschke, Fraunhofer-Institut für Kurzzeitdynamik Freiburg,
Ernst-Mach-Institut, Freiburg, Germany

Address: Tomasz Lekszycki, Warsaw University of Technology
and Department of Experimental Physiology and Pathophysiology, Medical University of Warsaw, Warsaw, Poland

---

Address: Ivan Giorgio, Sapienza University of Rome, Italy
and International Research Center for the Mathematics and Mechanics of Complex Systems, L'Aquila, Italy

---

Address: Emilio Turco, Universita Di Sassari
Dipartimento Di Architettura, Design e Urbanistica, Sassari, Italy

---

Address: Wolfgang H. Müller, Technische Universität Berlin,
Institut für Mechanik, Fachgebiet Kontinuumsmechanik und Materialtheorie, Berlin, Germany